Preparation and physico-chemical characteristics of luminescent apatite-based colloids

Ahmed Al-Kattan, Pascal Dufour, Jeannette Dexpert-Ghys, Christophe Drouet

Preparation and Physicochemical Characteristics of Luminescent Apatite-Based Colloids

Ahmed Al-Kattan,*,† Pascal Dufour,‡ Jeannette Dexpert-Ghys,§ and Christophe Drouet†

CIRIMAT Carnot Institute, University of Toulouse, CNRS/INPT/UPS, ENSIACET, 4 allée Emile Monso, BP 44362, 31432 Toulouse cedex 4, France, CIRIMAT Carnot Institute, University of Toulouse, CNRS/INPT/UPS, LCMIE, Université Paul Sabatier, 118 route de Narbonne, Bât. 2R1, 31062 Toulouse cedex 9, France, and CEMES 29, rue Jeanne Marvig, BP 94347, 31055 Toulouse cedex 4, France

Luminescent colloidal nanosystems based on europium-doped biomimetic apatite were prepared and investigated. The colloids were synthesized by soft chemistry in the presence of a phospholipid moiety, 2-aminoethylphosphoric acid (AEP), with varying europium doping rates. Physicochemical features, including compositional, structural, morphological, and luminescence properties, were examined. Experimental evidence showed that suspensions prepared from an initial Eu/(Eu + Ca) molar ratio up to 2% consisted of single-phased biomimetic apatite nanocrystals covered with AEP molecules. The mean particle size was found to depend closely on the AEP content, enabling the production of apatite colloids with a controlled size down to ca. 30 nm. The colloids showed luminescence properties typical of europium-doped systems with narrow emission bands and long luminescence lifetimes of the order to the millisecond, and the data suggested the location of Eu^{3+} ions in a common crystallographic environment for all the colloids. These systems, stable over time and capable of being excited in close-to-visible or visible light domains, may raise interest in the future in the field of medical imaging.

1. Introduction

Lanthanide-based phosphors have been used for many years in the field of optical devices (lasers, phosphors in color TV tubes, etc.)[1−3] and, more recently, for medical applications.[4−7] In particular, the development of luminescent probes in biology faces the issue of particle size,[8] especially when interactions with cells are foreseen, either in vitro or in vivo.[9−17]

Organic dyes, such as fluoresceine, green fluorescent protein, or rhodamine, are fluorescent probes commonly used in biology. However, these molecules do not allow an extended analysis of biological tissues due to fast damage under irradiation, as well as broad spectrum profiles and low photobleaching thresholds. To remedy this shortcoming, new classes of labeling agents, such as semiconductor quantum dots (e.g., CdSe-CdS, CdSe-ZnS, InAs), silica, or phosphate nanoparticles, were introduced more recently.[18−21] In particular, semiconductor systems show a higher photostability than usual organic fluorophores and a lower spectral width of emission, and their color can be adequately selected by modifying the particle size. These aspects have led many research groups to use quantum dots in biological assays.[20,21] However, the luminescence of these systems is accompanied by a flickering effect, leading to random appearance and disappearance of the luminescence, which limits the spatial resolution during bioluminescent analyses.[22,23] Also, semiconductors appear as rather toxic systems[24,25] due to the presence in their composition of Cd or As elements, for example.

Alternative routes for the preparation of other types of luminescent probes for a potential use in biology are still being explored. Lanthanide-doped inorganic nanoparticles have, for example, several advantages compared to quantum dots: their fluorescence is characterized by narrow emission bandwidths, and they show a high photochemical stability and a long fluorescence lifetime. Also, as for quantum dots, different colors are available by varying the luminescent center used (e.g., Tb, Eu, etc.). Increasing efforts have been focused on the production of luminescent nanoparticles doped with lanthanide(III) ions, such as lanthanum fluoride[26] and lanthanum phosphate,[27−30] or yttrium vanadate.[31,32] Favorable biological properties of such materials were reported in the last years.[18,33]

Nanocrystalline calcium phosphate apatites analogous to bone mineral, $Ca_{10-x}(PO_4)_{6-x}(HPO_4)_x(OH)_{2-x}$ ($0 \le x \le 2$), doped with lanthanide ions, such as Eu^{3+}, or Tb^{3+} have also been prepared.[33−36] The physicochemical characteristics and surface state of biomimetic apatites have largely been investigated, especially in view of bone regeneration applications.[37] Also, the ability of the apatite structure to accommodate many types of ionic substituents has been widely reported.[38,39] Some luminescence properties of Eu^{3+}-doped apatites were examined in several studies,[40−44] unveiling the possibility to obtain a red fluorescent probe. Moreover, the possibility to excite this ion at low energy (in or near the visible domain) may prove to be suitable for studying biological tissues.

Recently,[35] colloidal suspensions of apatite nanocrystals have been prepared in our laboratory for the setup of nanophosphors. However, the synthesis protocol used was based on precipitation from phosphoric acid and freshly calcined calcium oxide (under an inert atmosphere for avoiding the rehydration of CaO) and was thus hardly transposable to an industrial scale. The preparation of nonluminescent apatite colloids was then recently revisited in detail, revealing the possibility to obtain apatite colloids with controlled particle size, starting from nontoxic easily handled ionic salts.[45]

* To whom correspondence should be addressed. Phone: +33 (0)5 34 32 34 50 (A.A.), +33 (0)5 34 32 34 11 (C.D.). Fax: +33 (0)5 34 32 33 99 (A.A.), +33 (0)5 34 32 33 99 (C.D.). E-mail: ahmed.alkattan@ensiacet.fr (A.A.), christophe.drouet@ensiacet.fr (C.D.).

† CIRIMAT Carnot Institute, University of Toulouse, CNRS/INPT/UPS, ENSIACET.

‡ CIRIMAT Carnot Institute, University of Toulouse, CNRS/INPT/UPS, LCMIE, Université Paul Sabatier.

§ CEMES 29.

In the present work, we succeeded in preparing stable luminescent apatite colloids doped with a variable Eu/(Eu + Ca) molar ratio, starting from easily handled innocuous starting salts. The physicochemical characteristics of these colloids, including, in particular, the size, morphology, composition, and luminescence properties, were explored based on several complementary techniques.

2. Materials and Methods

2.1. Preparation of Apatite Colloids Doped with Europium. In this work, the preparation of colloidal apatite suspensions was based on the rapid coprecipitation at room temperature of calcium, europium, and phosphate salts. The synthesis was run in deionized water in the presence of a biocompatible stabilizing agent: 2-aminoethylphosphoric acid, "AEP" (under the form $NH_3^+-CH_2-CH_2-O-P(O)(O^-)_2$ at pH 9.5). After precipitation, the samples were aged at 100 °C for 16 h. AEP, a natural phospholipid moiety, was shown in previous studies to interact strongly with calcium ions[45−47] while providing an electrosteric repulsive effect, limiting apatite crystal agglomeration. Unless otherwise specified, the starting AEP/(Ca + Eu) molar ratio was set to 1. This value has been shown[45] to lead to stable deagglomerated apatite particles with a mean particle size around 30 nm. The effect of AEP content was also followed. To this purpose, some suspensions were prepared starting from a AEP/(Ca + Eu) ratio of 0.8, 0.6, 0.4, and 0.2.

For each preparation, three solutions were prepared. Solution (A) contained a total of 4.87 mmol of calcium nitrate ($Ca(NO_3)_2 \cdot 4H_2O$) and europium nitrate ($Eu(NO_3)_3 \cdot 6H_2O$) with a variable Eu/(Eu + Ca) molar ratio in the initial reaction mixture (0, 1.5, 2, 4, 7, 10, and 100%), dissolved in deionized water. Solution (B) contained 4.87 mmol of AEP in deionized water. Finally, solution (C) was prepared by dissolving 1.62 mmol of di-ammonium hydrogen phosphate in deionized water, with an initial molar ratio (Ca + Eu)/P of 0.33. This ratio was used previously for the preparation of apatite colloids in the presence of AEP.[45]

In a typical procedure, solution (A) was mixed with solution (B) under constant stirring. The acidic pH of the resulting solution, referred to as solution (D), as well as that of solution (C) was adjusted to 9.5 by addition of ammonia. Such an alkaline pH value was selected in order to favor the precipitation of an apatite phase close to stoichiometry, which exhibits good chemical stability.[45] The pH of the colloids can be adjusted after synthesis to a physiological value prior to biological applications. The transparent colloids obtained after aging were purified by dialysis in water to remove unreacted salts (cellulose membrane, cutoff 6000−8000 Da). Ultracentrifugation at 50 000 rounds/min, and with 3 successive washing steps in deionized water, was also occasionally used as an alternative purification process for cross-checking. No differences were evidenced between ultracentrifuged and dialyzed samples.

For comparative purposes, "reference" noncolloidal apatite suspensions were also synthesized using a similar protocol as above, but without addition of AEP. In this case, solution (B) contained only deionized water.

In all cases, a part of the suspensions was freeze-dried in view of the physicochemical powder characterization.

2.2. Physicochemical Characterization. Calcium and europium contents were determined by induced coupled plasma atomic emission spectroscopy, ICP-AES (relative uncertainty = 3%). The amount of mineral phosphate (from apatite) in the samples was determined by colorimetry at $\lambda = 460$ nm, using the yellow phospho-vanado-molybdenum complex[48] (relative uncertainty = 0.5%). The AEP content in the stable colloids was drawn from nitrogen microanalysis (relative uncertainty = 0.4%).

The crystallographic structure of the powders obtained for varying europium doping rates and after freeze-drying was investigated by way of X-ray diffraction (XRD) using a CPS 120 INEL diffractometer with the Kα1 cobalt radiation (λ = 1.78892 Å).

Fourier transform infrared (FTIR) analyses were performed on a Nicolet 5700 spectrometer, in the wavenumber range of 400−4000 cm^{-1} with a resolution of 4 cm^{-1}. Raman spectra were recorded on a Jobin Yvon HR 800 spectrometer, with a laser excitation wavelength of 632.8 nm.

The size and morphology of the apatite nanocrystals were followed by transmission electron microscopy (TEM) on a JEOL JEM-1011 set at 100 keV. The experiments were conducted on the purified colloidal suspensions. For these TEM observations, the suspensions were briefly sonicated (50 kHz, 30 s) and the carbon-coated copper TEM grids were rapidly dipped into the suspension and allowed to dry prior to analysis.

The particle size (hydrodynamic diameter, D_h) of the colloids prepared was determined by dynamic light scattering (DLS) with a Nanosizer ZS apparatus from Malvern Instruments ($\lambda = 630$ nm). The dispersion of the data points is estimated to 0.5%. These experiments were carried out on nondialyzed suspensions so as to provide high ionic strength, giving D_h values close to geometrical particle sizes and thus leading to fully exploitable DLS measurements. Punctual zeta potential measurements were also made, as mentioned in the text, using this apparatus.

The luminescence properties of the colloids were investigated using a Horiba Jobin Yvon Fluorolog 3-11 spectrofluorometer equipped with a 450 W xenon lamp. Excitation and emission were measured at room temperature directly on the colloidal suspensions, after dialysis.

Excitation spectra were recorded between 350 and 600 nm, monitoring the $^5D_0 \rightarrow {}^7F_2$ emission of Eu^{3+} at $\lambda_{em} = 612$ nm (spectral bandwidth = 2 nm). Emission spectra were recorded in the 500−700 nm range, with a spectral bandwidth of 1 nm, under selected excitation in the $^7F_0 \rightarrow {}^5L_6$ transition of Eu^{3+} at $\lambda_{ex} = 392.8$ nm or in the $^7F_0 \rightarrow {}^5D_2$ transition at $\lambda_{ex} = 464.2$ nm.

The transient characteristics of the emitting level $^5D_0$ of Eu^{3+} were investigated with the phosphorimeter FL-1040, equipped with a UV xenon flash tube. Emission decays were analyzed at chosen λ_{ex} and λ_{em} on a time interval of 3.5 ms. The time resolution imposed by the apparatus in the experimental conditions employed is 30 μs.

3. Results and Discussion

3.1. Physicochemical Characterization. Several apatite suspensions were prepared in the presence of AEP with increasing europium contents corresponding to initial Eu/(Eu + Ca) molar ratios of 0, 1, 1.5, 2, 2.5, 4, 7, 10, and 100%. The suspensions prepared from initial ratios lower than 2.5% were translucent colloids, highly stable over time (greater than 6 months). In contrast, beyond this initial europium content in the solution, a noticeable increase of the suspension viscosity was observed, leading to a rapid sedimentation in the case of 100%.

The XRD patterns obtained on the purified freeze-dried suspensions are reported in Figure 1. The patterns corresponding to molar ratios in the initial reaction mixture up to 2.5% clearly exhibit diffraction peaks characteristic of an apatite structure, and no additional crystallized phase could be detected. Ad-

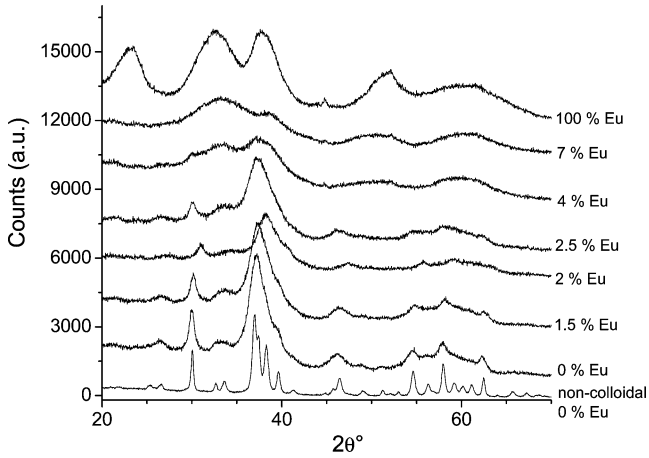

Figure 1. XRD patterns for apatite colloids prepared with increasing Eu/(Ca + Eu) initial molar ratios and for a noncolloidal reference (AEP-free).

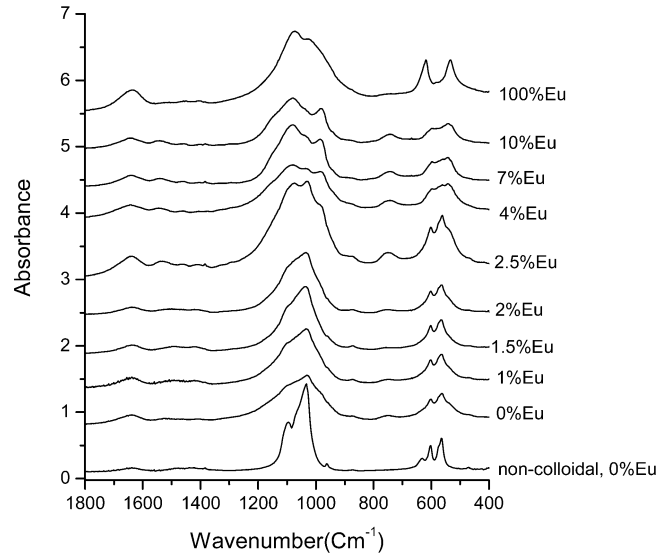

Figure 2. FTIR spectra for apatite colloids prepared with increasing Eu/(Ca + Eu) initial molar ratios and for a noncolloidal reference (AEP-free).

ditionally, the crystallinity state of these samples was found to decrease with increasing Eu contents in the initial mixture, which is, for example, visible in the 2θ ranges of 35−41° and 53−63°. This point probably unveils some inhibitory effect of europium on apatite crystal growth, as already evidenced for other ions.[49] A similar inhibitory effect of AEP molecules can also be seen by comparing the 0% Eu colloidal suspension to its noncolloidal AEP-free counterpart (see Figure 1), which is in agreement with a previous report for AEP-containing apatite colloids.[45]

On the contrary, for initial Eu/(Eu + Ca) molar ratios greater than 2.5%, a drastic modification of the XRD pattern was seen, and apatite could no more be detected in these systems, which were found to approach the structure of europium phosphate (comparison to JCPDS card No. 20-1044 relative to $EuPO_4 \cdot H_2O$), despite a poor crystallinity state. Chemical analyses performed on the sample corresponding to 100% Eu revealed a Eu/PO_4 molar ratio close to unity (experimental value = 0.96), therefore, corroborating the hypothesis of europium phosphate formation in this case.

FTIR spectra were then recorded on the purified freeze-dried samples corresponding to the varying europium doping rates (Figure 2). For initial Eu/(Eu + Ca) molar contents between 0 and 2%, the characteristic absorption bands of apatite were observed, especially around 1095, 1033, 601, and 563 cm^{-1}, assigned to the PO_4^{3-} ν_3 and ν_4 vibration modes. The peak observed around 875 cm^{-1} can be assigned to HPO_4^{2-} ions. The broad bands observed are, however, only moderately well-defined, with a decreasing resolution as the europium doping rate increases, which can be related to a rather low crystallinity state, in accordance with the XRD findings. The apatitic nature of the phase in presence was also checked by Raman spectroscopy as the characteristic PO_4^{3-} ν_1 band was observed at 961 cm^{-1}.

In contrast, the FTIR spectra obtained for Eu/(Eu + Ca) ratios greater than 4% exhibit sharp alterations, revealing strong modifications for elevated europium contents. In particular, the spectrum recorded for 100% Eu, with pronounced bands at 538, 628, and 1082 cm^{-1}, was found to be characteristic of hydrated europium phosphate; this was checked by comparison with a reference $EuPO_4.H_2O$ compound prepared by precipitation at room temperature from europium chloride and ammonium dihydrogen phosphate. The sample prepared with a Eu/(Eu + Ca) ratio of 2.5% was found to be in an intermediary situation, with apatite obviously present beside europium phosphate. This observation indicates that a finer analysis can be drawn from FTIR data as compared to XRD results where the presence of europium phosphate could hardly be detected for the sample corresponding to the initial Eu/(Eu + Ca) ratio of 2.5% Eu.

The examination of the FTIR spectra for the single-phased systems corresponding to initial Eu/(Eu + Ca) ratios ranging from 0 to 2% also showed the presence of additional peaks, in particular, at 754 cm^{-1}. These bands are not assignable to apatite nor to europium phosphate. These additional features can be unambiguously linked to the presence of AEP molecules in the colloids, in the form of $Ca(AEP)_2$, as was shown earlier.[45] These findings thus unveil the existence of $Ca^{2+}(AEP^-)_2$ complexes on the surface of the apatite nanocrystals, as was previously shown for europium-free apatite colloids.[45]

Chemical analyses were carried out on the purified samples corresponding to Eu/(Eu + Ca) starting ratios from 0 to 2%. The final Eu/(Eu + Ca) ratios in the colloids were then found in the range of 0−2.9 atomic %. The Ca, Eu, and mineral phosphate contents were quantified, enabling us to evaluate the overall (Ca + Eu)/P ratio of the colloids. This ratio was found in all cases between 1.35 and 1.50. These values are noticeably lower than the value of 1.67 corresponding to stoichiometric hydroxyapatite; they, therefore, point out the nonstoichiometric nature of the apatite phase, thus confirming its biomimetic nature.

The possibility to incorporate europium in the apatite structure has already been mentioned by several authors,[42,44,45] although generally for apatite compounds prepared at higher temperature. Several substitution mechanisms can be considered[43] for explaining the incorporation of Eu^{3+} ions in Ca^{2+} sites. In the absence of monovalent or tetravalent ions in the medium, four distinct mechanisms can be distinguished: the replacement of three Ca^{2+} by two Eu^{3+} (mechanism no.1), the deprotonation of some HPO_4^{2-} ions into PO_4^{3-} (mechanism no. 2), and the additional incorporation of OH^- (mechanism no. 3) or of oxygen O^{2-} ions (mechanism no. 4). The existence of oxygen ions O^{2-} in Eu-doped apatites, as involved in mechanism no. 4, has indeed been reported and should thus not be a priori discarded.[42−44] It should be noted that a combination of two or more of these mechanisms may also be involved. To investigate some more the Eu incorporation mechanism, a series of noncolloidal apatite suspensions were prepared in similar conditions, but in the

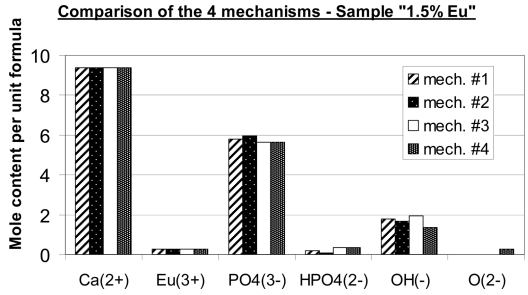

Figure 3. Chemical composition for the 1.5% Eu sample (starting doping rate) evaluated from the four different incorporation mechanisms.

absence of AEP in the medium. Again, increasing Eu contents in the range of 0−2% were considered. After chemical analyses were performed on several specimens of each sample, the (Ca + Eu)/P molar ratio of the apatite phase was evaluated for these noncolloidal samples. The results obtained pointed out a slight decrease of this ratio upon Eu incorporation: typically from 1.66 down to 1.57 for Eu starting doping rates increasing from 0 to 2%. Based on the knowledge of Eu/(Ca + Eu) and (Ca + Eu)/P ratios for the 0, 1, 1.5, and 2% Eu samples, one can thus estimate their chemical composition by considering consecutively each of the four possible incorporation mechanisms. Interestingly, these determinations indicated that all four mechanisms remained possible for explaining the incorporation of Eu^{3+} ions in Ca^{2+} sites. This is, for instance, exemplified in Figure 3 in the case of the sample corresponding to a starting doping rate of 1.5% Eu. A preferential mechanistic scheme thus cannot be derived at this point. It should also be noted that the preferential mechanistic scheme for Eu incorporation may depend, to some extent, on the doping rate. The observation of a maximum limit of Eu incorporation does not seem to be directly explainable based only on mechanistic considerations: this limit probably originates from other factors, such as thermodynamically driven destabilization of the system, possibly linked to differences between Eu−O and Ca−O bond lengths. Additional work specifically dedicated to examine these aspects will be needed to investigate this point, which lies beyond the scope of the present paper. Although the presence of AEP in the colloidal synthesis route leads to less-crystallized apatite phases, linked to some inhibitory effect of AEP pointed out from XRD analyses, it seems reasonable to expect a similar situation in terms of Ca/Eu substitution.

The amount of AEP contained in the colloids was determined from the amount of nitrogen titrated by way of elemental microanalyses. The AEP content was found to represent 8−11 wt % of the colloidal particles, leading to an AEP/apatite molar ratio in the range of 0.7−0.8. It is interesting to note that this ratio is lower than the one observed by Bouladjine et al.[45] for europium-free apatite colloids prepared at 80 °C. These findings can probably be explained by the differences existing in the synthesis protocols used in the two studies, especially in terms of starting ionic concentrations and aging temperatures. The location of the AEP molecules on the surface of the apatite crystals was evidenced by Bouladjine et al.[45] who showed the positive surface charge of the colloids obtained in the presence of AEP and the decrease in size upon increasing the AEP content. Interestingly, the zeta potential of the colloids prepared in the present work was also found to be clearly positive (e.g., +12.4 mV for the sample corresponding to the initial doping of 1.5% Eu), thus showing again the exposure of the ammonium groups $-NH_3^+$ from AEP molecules toward the solution. Also, a decrease of the initial AEP concentration provoked a sedimentation phenomenon for AEP/(Ca + Eu) ratios lower than 0.2, whereas stable colloidal suspensions were obtained beyond 0.4. This sedimentation can then most probably be explained by an insufficient electrosteric repulsion between adjacent particles when the surface content in AEP molecules decreases beyond a limit value.

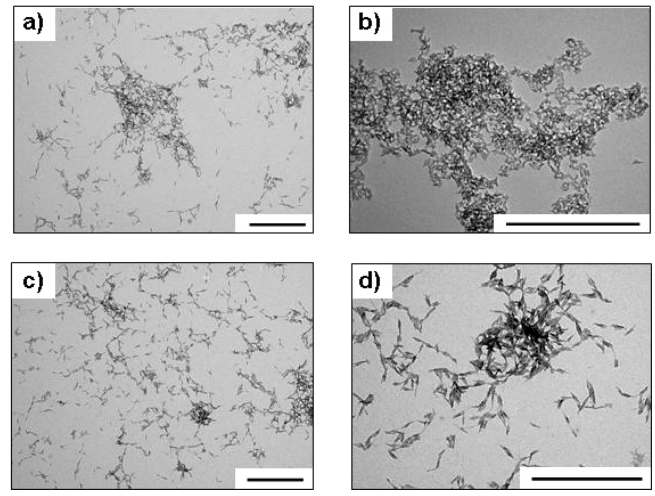

Figure 4. TEM observations (scale bar = 500 nm) of the apatite colloids with Eu/(Ca + Eu) initial ratios of 0% (a, b) and 1.5% (c, d), prepared from AEP/(Ca + Eu) = 1.

Transmission electron microscopy (TEM) observations were performed on the dialyzed colloids in order to inspect the constitutive nanocrystals within the colloidal particles. In a first step, the study was conducted on colloidal suspensions with Eu contents ranging from 0 to 1.5% (prepared with an initial ratio AEP/(Ca + Eu) = 1) to study the effect of the introduction of Eu^{3+} ions into the mineral host matrix. TEM observations showed no obvious differences when varying the europium content (see Figure 4) for samples doped with 0 and 1.5% Eu. In all cases, the micrographs recorded at low magnification revealed very homogeneous crystal aspects with an ellipsoidal morphology and with dimensions around 28 nm in length and 9 nm in width. These observations attest that the introduction of europium in this Eu/(Ca + Eu) range has no obvious impact on the size and morphology of the individual nanocrystals constituting the colloidal particles.

In a second step, the effect of a change of the initial AEP/(Ca + Eu) ratio in the range of 0.4−1 was followed by TEM in order to inspect the possible influence of the amount of AEP on the size and aspect of individual nanocrystals. The results obtained showed (Figure 5) very similar features for AEP/(Ca + Eu) = 0.4, 0.6, and 1, indicating that the presence of AEP in these conditions did not affect noticeably the size and aspect of the individual apatite nanocrystals.

Numerous studies have, however, shown the general tendency of apatite nanocrystals to agglomerate. Although TEM observations showed no impact of the presence of AEP molecules on the size of the constitutive nanocrystals, differences in the agglomeration state may occur, as was already observed for europium-free samples.[45] To determine the size of the colloidal particles obtained and to follow, thereby, the agglomeration state of apatite, granulometry measurements were carried out on the colloids by dynamic light scattering (DLS), leading to hydrodynamic radii, D_h.

The results (Figure 6) showed that, for initial AEP/(Ca + Eu) ratios between 1 and 0.6, the hydrodynamic diameter (D_h) was close to 30 nm. This value is very close to the individual crystal

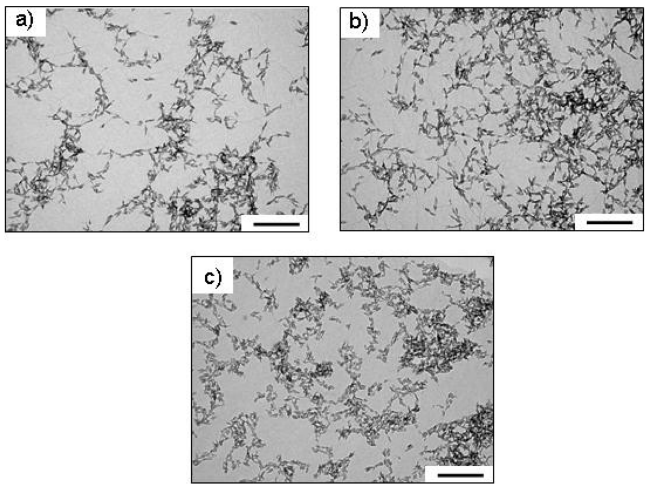

Figure 5. TEM observations (scale bar = 200 nm) of apatite colloids doped with Eu/(Ca + Eu) initial molar ratios at 1.5% and AEP/(Ca + Eu) = 0.8 (a), 0.6 (b), and 0.4 (c).

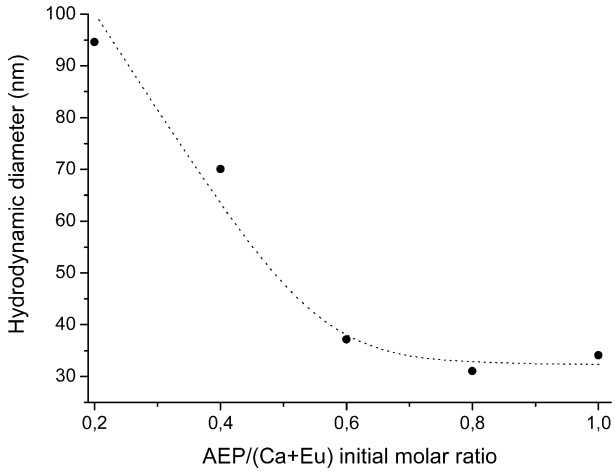

Figure 6. Effect of the AEP/(Ca + Eu) initial molar ratio on the hydrodynamic diameter of colloidal particles.

size estimated from TEM, indicating that, for these AEP contents, the crystal agglomeration is extremely limited. These findings can most probably be explained by the strong electrosteric repulsive effect induced by the presence of an important amount of AEP on the surface of the apatite nanocrystals. In contrast, for decreasing AEP/(Ca + Eu) ratios from 0.6 to 0.2, the value of D_h increased rapidly up to about 95 nm. Such sizes, greater than the ones measured for individual crystals by TEM, unveil an increased agglomeration state of the apatite nanocrystals when the amount of AEP decreases: the presence of these molecules controls the agglomeration state of the colloidal particles. In other words, the particle size for such apatite colloids may be tailored by varying the synthesis conditions.

3.2. Luminescence Properties. The luminescence properties of the colloids prepared in this work were then investigated.

Excitation spectra were first recorded by monitoring the red luminescence intensity at 612 nm (main emission line). The maximum emission was found for an excitation performed at 392.8 nm, a wavelength close to the visible light domain. This wavelength corresponds to the direct excitation of Eu^{3+} ions from the ground state $^7F_0$ to the $^5L_6$ excited level: it is usually the most intense of the intraconfiguration absorption lines of Eu^{3+} ($4f^6$ configuration).

As expected, a secondary excitation peak, although less intense, is also observed at 464.2 nm. This peak is assignable

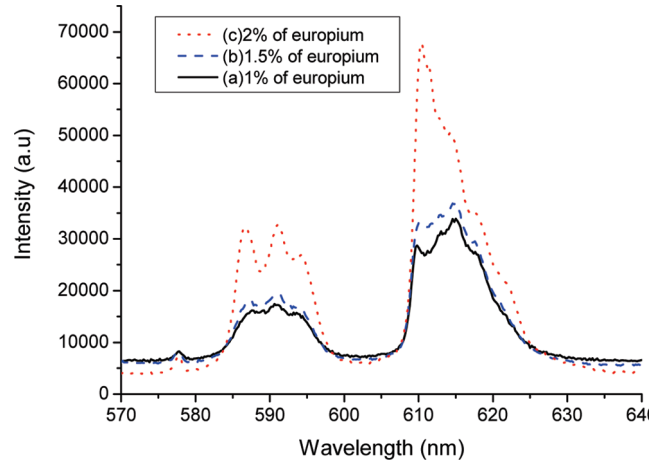

Figure 7. Emission spectra of apatite colloids doped with Eu/(Ca + Eu) initial molar ratios of 1% (a), 1.5% (b), and 2% (c) of europium Eu^{3+} under excitation at 392.8 nm.

to the $^7F_0 \rightarrow {}^5D_2$ absorption and lies within the visible domain. These observations show the possibility to use such luminescent nanoprobes for studying biological tissues because they only require low-energy excitation, preventing the deterioration of live cells.

Luminescence emission spectra were then recorded for suspensions corresponding to the starting Eu/(Eu + Ca) ratios of 1, 1.5, and 2%, under excitation at 392.8 nm (Figure 7). The observed spectral features are easily ascribed to the 4f−4f transition within the $4f^6$ configuration of Eu^{3+}. In all cases, three domains can be distinguished: 575−580 nm, 583−603 nm, and 605−627 nm, corresponding, respectively, to the transitions $^5D_0 \rightarrow {}^7F_0$, $^5D_0 \rightarrow {}^7F_1$, and $^5D_0 \rightarrow {}^7F_2$ characteristic of the Eu^{3+} ion. Also, the global emission intensity was found to increase noticeably with the level of europium doping.

The $^5D_0 \rightarrow {}^7F_0$ transition located at 578 nm has been studied, in particular, because the energy levels $^5D_0$ and $^7F_0$ are both nondegenerated, meaning that only a single peak for the $^5D_0 \rightarrow {}^7F_0$ transition should appear if all the Eu^{3+} ions were in the same crystal field environment. Besides, the maximum numbers of emission lines are three and five per crystal field environment for $^5D_0 \rightarrow {}^7F_1$ and $^5D_0 \rightarrow {}^7F_2$, respectively. For all three cases, only one component is recorded for $^5D_0 \rightarrow {}^7F_0$, then three distinct components for $^5D_0 \rightarrow {}^7F_1$, and four or five for $^5D_0 \rightarrow {}^7F_2$, with a considerable overlapping of the lines, due to inhomogeneous broadening as it is usual in poorly crystallized samples.

It is, however, worth mentioning that, for the suspension obtained from an initial Eu/(Eu + Ca) ratio of 2%, a significant change was observed for each transition as compared with the other two suspensions. The intensity of luminescence was found to notably increase, and as a general observation, the lines are narrower than for the two other samples. Moreover, the overall shape of $^5D_0 \rightarrow {}^7F_2$ is modified with relatively more intensity at 610 and at 624 nm. These findings indicate that the immediate chemical environment of europium in this colloid is partly different from the environment found in the other two suspensions. To shed some light on this aspect, luminescence emission spectra of $EuPO_4 \cdot H_2O$ and $Eu(OH)_3$ reference compounds were recorded and compared with the emission spectrum of the 2% Eu suspension (Figure 8). The spectra being poorly resolved, it may not be concluded if one or the other of the two phases appears exclusively in the 2% colloid: more probably, a mixture of both is present, beside the apatite, in this sample.

Such observations show that luminescence spectroscopy proves to be an interesting complementary tool for sample

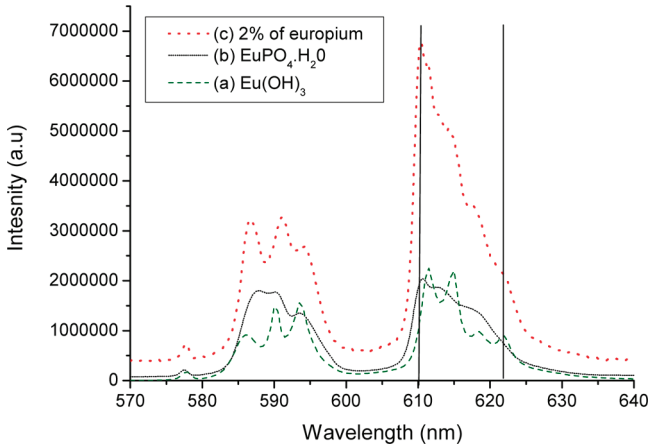

Figure 8. Emission spectra of a Eu^{3+}-doped apatite colloid with a Eu/(Ca + Eu) initial molar ratio of 2% (a) and for reference compounds $EuPO_4 \cdot H_2O$ (b) and $Eu(OH)_3$ (c), under excitation at 392.8 nm.

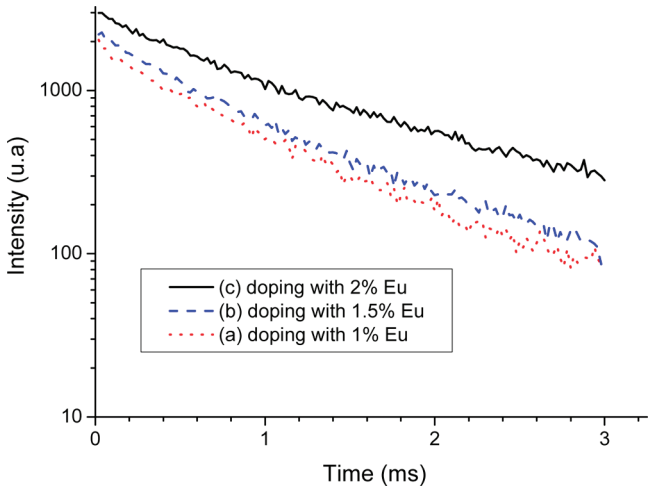

Figure 9. Luminescence decay profiles of the $^5D_0$ (Eu^{3+}) level for three apatite colloids: 1% (a), 1.5% (b), and 2% (c), under excitation at 392.8 nm and at ambient temperature.

characterization, exploiting europium as an internal probe. Indeed, the presence of traces of such secondary phases had only been suggested from FTIR analyses beyond a starting Eu/(Ca + Eu) ratio of 2.5%.

The luminescence lifetime of the europium $^5D_0$ level measured on the same set of samples was also studied, and Figure 9 displays the decays observed for suspensions corresponding to an initial Eu/(Eu + Ca) ratio of 1, 1.5, and 2%. As observed on the spectra, it may be noticed that the decays for 1% and 1.5% Eu are essentially the same, whereas for 2% Eu, the emission decays more slowly. In the figure (Figure 9), the I(t) curves have been displayed on a logarithmic scale, showing that they are not purely monoexponential. We have, nevertheless, measured the average decay time τ as the time for which $I(\tau) = I_0/\exp(1)$, leading to 0.73 ± 0.03 ms for 1% or 1.5% Eu and 1.00 ± 0.05 ms for 2% Eu. This observation may be linked to the above results, suggesting the presence of secondary phases beside apatite for this sample, leading to modified luminescence properties.

It is interesting to note that, in all cases, the luminescence exponential decay was found to be of the order to the millisecond. This order of magnitude is customary, in the case of lanthanide-doped systems, due to the intrinsic properties of Ln^{3+} luminescent centers, and it enables one to envision applications as luminescent nanoprobes for biological applications because the autofluorescence of the biological medium exhibits a luminescence decay time of the order of nanoseconds. In a second step, the luminescence properties, both in terms of excitation/emission and lifetime, of colloidal suspensions obtained at constant europium content (initial doping = 1.5% Eu), but from varying initial amounts of AEP in the medium, were followed. AEP/(Ca + Eu) molar ratios of 0.4, 0.6, 0.8, and 1 were tested. The results obtained indicated that no obvious differences could be noticed between the three suspensions, suggesting that the chemical environment of europium was essentially unchanged.

4. Conclusions

Europium-doped calcium phosphate apatite-based colloids were produced in the presence of a phospholipid moiety, 2-aminoethylphosphoric acid (AEP), with varying europium doping rates, and their physicochemical characteristics were investigated in detail. The experimental data obtained for suspensions prepared from an initial Eu/(Ca + Eu) molar ratio up to 2% converge to indicate that these colloids consist of biomimetic apatite nanocrystals covered with AEP molecules. Moreover, the agglomeration state of apatite crystals was found to be closely dependent on the amount of AEP in the system, and the mean particle size can be tailored between 30 and 100 nm. The colloidal suspensions as prepared were found to be stable over time beyond at least 6 months.

The luminescence properties of these nanoprobes were analyzed in terms of excitation, emission, and lifetime. The typical luminescence features of europium-doped systems were witnessed, with narrow emission peaks and long luminescence lifetimes. Our observations support the location of europium in a common crystallographic environment for all the colloids prepared.

The potential of such systems in the field of optical imaging related to biology will then have to be investigated.

Supporting Information Available: Emission spectra of apatite colloids doped with Eu/(Ca + Eu) initial molar ratios of 1, 1.5, and 2% Eu under excitation at 392.8 nm; luminescence decay profiles of the $^5D_0$ (Eu^{3+}) level for three apatite colloids—1, 1.5, and 2% Eu—under excitation at 392.8 nm and at ambient temperature; and TEM micrograph for apatite colloids prepared from Eu/(Ca + Eu) = 1.5%. This material is available free of charge via the Internet at http://pubs.acs.org.

References and Notes

(1) Görller-Warlrand, C.; Binnemans, K. In *Handbook on the Physics and Chemistry of Rare Earths*; Gschneidner, K. A., Eyring, L., Eds.; North-Holland: Amsterdam, 1998; Chapter 167.

(2) Franz, K. A.; Kethr, W. G.; Siggle, A.; Wiieczoreck, J. In *Ullmann's Encyclopedia of Industrial Chemistry*; Elvers, B., Hawkins, S., Schulz, G., Eds.; VCH: Weinheim, Germany, 1985; Chapter A15.

(3) Heyes, A. L.; Seefeldt, S.; Feist, J. P. *Opt. Laser Technol.* **2006**, *38*, 257–265.

(4) Diamente, P. R.; Burk, R. D.; Van Veggel, F. C. *Langmuir* **2006**, *22*, 1782–1788.

(5) Selvin, P. R. *Annu. Rev. Biophys. Biomol. Struct.* **2002**, *31*, 275–302.

(6) Huhtinen, P.; Vaarno, J.; Soukka, T.; Lövgren, T.; Haïrmaï, H. *Nanotechnology* **2004**, *15*, 1708–1715.

(7) Gao, X.; Cui, Y.; Levenson, R. M.; Chung, L. W. K.; Nie, S. *Nat. Biotechnol.* **2004**, *22*, 969–976.

(8) Wang, C. W.; Moffitt, M. G. *Langmuir* **2005**, *21*, 2465–2473.

(9) Stella, B.; Arpicco, S.; Peracchia, M. T.; Desmaele, D.; Hoebeke, J.; Renoir, M.; D'Angelo, J.; Cattel, L.; Couvreur, P. *J. Pharm. Sci.* **2000**, *89*, 1452–1464.

(10) Mitra, S.; Gaur, U.; Ghosh, P. C.; Maitra, A. N. *J. Controlled Release* **2001**, *74*, 317–323.

(11) Allemann, E.; Gurny, R.; Doelker, E. *Eur. J. Pharm. Biopharm.* **1993**, *39*, 91–173.
(12) Kohler, N.; Fryxell, G. E.; Zhang, M. *J. Am. Chem. Soc.* **2004**, *126*, 7206–7211.
(13) Zuber, G.; Zammut-Italiano, L.; Dauty, E.; Beher, J. P. *Angew. Chem.* **2003**, *42*, 2666–2669.
(14) Drumond, D.; Meyer, C.; Hong, O.; Kirpotin, K.; Papahadjopoulos, D. *Pharmacol. Rev.* **1999**, *51*, 691–743.
(15) Dubé, D.; Francis, M.; Leroux, J. C.; Winnik, F. M. *Bioconjugate Chem.* **2002**, *13*, 685–692.
(16) Mohapatra, S.; Mallick, S. K.; Maiti, T. K.; Ghosh, S. K.; Paramanik, P. *Nanotechnology* **2007**, *18*, 1–9.
(17) Battacharya, R.; Ranjan Patra, C.; Earl, A.; Wang, S.; Katraya, A.; Lu, L.; Kizhakketdarthu, J. N.; Yaszemski, M. J.; Greipp, P. R.; Mukhhopadhyay, D.; Mukherjee, P. *Nanomedicine* **2007**, *3*, 224–238.
(18) Meiser, F.; Cortez, C.; Caruso, F. *Angew. Chem.* **2004**, *43*, 5954–5957.
(19) Ow, H.; Larson, D. R.; Srivastava, M.; Baird, B. A.; Webb, W. W.; Weisner, U. *Nano Lett.* **2005**, *5*, 113–117.
(20) Parak, W. J.; Gerion, D.; Pellegrino, T.; Zanchet, D.; Micheel, C.; Williams, S. C.; Boudreau, R.; Le Gros, M. A.; Larabel, C. A.; Alivisatos, A. P. *Nanotechnology* **2003**, *14*, R15–R17.
(21) Bruchez, M.; Moronne, M.; Gin, P.; Weiss, S.; Alivisatos, A. P. *Science* **1998**, *281*, 2013–2016.
(22) Shimizu, K. T.; Neuhauser, R. G.; Leatherdale, C. A.; Empedocles, S. A.; Woo, W. K.; Bawendi, M. G. *Phys. Rev. B* **2001**, *63*, 205–316.
(23) Brokmann, X.; Hermier, J. P.; Messin, G.; Desbiolles, P.; Bouchaud, J. P.; Dahan, M. *Phys. Rev. Lett.* **2003**, *90*, 120601.
(24) Ballou, B.; Lagerholm, B. C.; Ernst, L. A.; Bruchez, M. P.; Waggoner, A. S. *Bioconjugate Chem.* **2004**, *15*, 79–86.
(25) Derfus, A. M.; Chan, W. C. W.; Bhatia, S. N. *Nano Lett.* **2004**, *4*, 11–18.
(26) Wang, F.; Zhang, Y.; Fan, X.; Wang, M. *J. Mater. Chem.* **2006**, *16*, 1031–1034.
(27) Meyssamy, H.; Riwotzki, K.; Kornowski, A.; Naused, S.; Haase, M. *Adv. Mater.* **1999**, *11*, 840–844.
(28) Riwotzki, K.; Meyssamy, H.; Kornowski, A.; Haase, M. *J. Phys. Chem. B* **2000**, *104*, 2824–2828.
(29) Riwotzki, K.; Meyssamy, H.; Schnablegger, H.; Kornowski, A.; Haase, M. *Angew. Chem.* **2001**, *40*, 573–576.
(30) Schuetz, P.; Caruso, F. *Chem. Mater.* **2002**, *14*, 4509–4516.
(31) Huignard, A.; Buissette, V.; Franville, A. C.; Gacoin, T.; Boilot, J. P. *J. Phys. Chem. B* **2003**, *107*, 6754–6759.
(32) Huignard, A.; Gacoin, T.; Boilot, J. P. *Chem. Mater.* **2000**, *12*, 1090–1094.
(33) Padilla Mondéjar, S.; Kovtun, A.; Epple, M. *J. Mater. Chem.* **2007**, *17*, 4153–4159.
(34) Doat, A.; Pellé, F.; Gardant, N.; Lebugle, A. *J. Solid State Chem.* **2004**, *117*, 1179–1187.
(35) Chane-Ching, J. Y.; Lebugle, A.; Rousselot, I.; Pourpoint, A.; Pellé, F. *J. Mater. Chem.* **2007**, *17*, 2904–2913.
(36) Fanjul, M.; Doat, A.; Pellé, F.; Hollande, E.; Lebugle, A. *In Vitro Cell. Dev. Biol.* **2004**, *40*, 81A.
(37) Legeros, R. Z. *Prog. Cryst. Growth Charact.* **1981**, *4*, 1–45.
(38) Cazalbou, S.; Eichert, D.; Ranz, X.; Drouet, C.; Combes, C.; Harmand, M. F.; Rey, C. *J. Mater. Sci.: Mater. Med.* **2005**, *16*, 405–409.
(39) Rey, C.; Combes, C.; Drouet, C.; Sfihi, H.; Barroug, A. *Mater. Sci. Eng., C* **2007**, *27*, 198–205.
(40) Doat, A.; Fanjul, M.; Pellé, F.; Holland, E.; Lebugle, A. *Biomaterials* **2003**, *24*, 3365–3371.
(41) El Ouenzerfi, R.; Kbir-Ariguib, N.; Trabelsi-Ayedi, M.; Piriou, B. *J. Lumin.* **1999**, *85*, 71–77.
(42) Ternane, R.; Trabelsi-Ayedi, M.; Kbir-Ariguib, N.; Piriou, B. *J. Lumin.* **1999**, *81*, 165–170.
(43) Martin, P.; Carlot, G.; Chevarier, A.; Den-Auwer, C.; Panczer, G. *J. Nucl. Mater.* **1999**, *275*, 268–276.
(44) Eun Jin, K.; Sung-Woo, C.; Seong-Hyeon, H. *J. Am. Chem. Soc.* **2007**, *90*, 2795–2798.
(45) Bouladjine, A.; Al-kattan, A.; Dufour, P.; Drouet, C. *Langmuir* **2009**, *25*, 12256–12265.
(46) Rothfield, L.; Finkelstein, A. *Annu. Rev. Biochem.* **1968**, *37*, 463–495.
(47) Bissinger, P.; Kumberger, O.; Schier, A. *Chem. Ber.* **1991**, *124*, 509–513.
(48) Gee, A.; Dietz, V. R. *Anal. Chem.* **1953**, *25*, 1320–1324.
(49) Blumenthal, N. C. *Clin. Orthop. Relat. Res.* **1989**, *247*, 279–289.